VALIDATION OF A TIP FEEDBACK SENSOR BASED FLEXIBLE MANIPULATOR MODEL

J WARRINK & A. S. WHITE

School of Computing Science
Middlesex University
Trent Park
Bramley Rd.
London N14 4YZ
United Kingdom
Email a.white@mdx.ac.uk

Abstract. This paper describes the simulation of a flexible robot link, which is programmed in ACSL; a Fortran based simulation language. The simulation of this flexible link manipulator is based on the finite difference solution of a Lagrange-Euler formulation. The effects of stiction torque have been included in an existing simulation to improve the simulation step response compared with the prototype especially for the case of different directions and payloads.The manipulator was controlled by classical PD and Fuzzy PD controllers. The step responses of the simulation before and after the changes in the model were validated through correlation coefficients and the characteristics of the simulation responses. It was shown that the correlation coefficient of the simulation is greater than 78% without the effect of stiction torque and that the parameter changes can improve the overshoot performance of the simulation to 94% in one direction. Simulation with the fuzzy controller can achieve correlation coefficients of 99% without payload.

Keywords Simulation, flexible manipulator, Validation, ACSL, MATLAB, Tip feedback sensor

1.0 ROBOT SYSTEM

This section gives a description of the prototype of the robot arm and its' simulation. This arm control system was developed to enable very large and hence flexible links to be used in the nuclear industry. To provide a challenging test for the chosen fuzzy controller a very poor mechanical structure was designed. It had a flexible arm, with a lowest natural frequency of 16.5 Hz, bolted joints and considerable friction in the bearings. This work describes some of the validation of the simulation model to enable a fuzzy controller to be designed. It did prove to be very challenging to gain a sufficiently accurate model. Early work showed poor models and it took a long careful series of experiments to highlight the defects of the range of models used. This paper illustrates the validation of the effects of the stiction component of the bearing friction. The purpose of the experiments decsribed here is to detail a coherent model of a very flexible arm driven by a control system that was non-linear and show what features in the range of models that could be explained and those that could not.

1.1 The Prototype

A laser beam (figure 1) directs the arm tip's

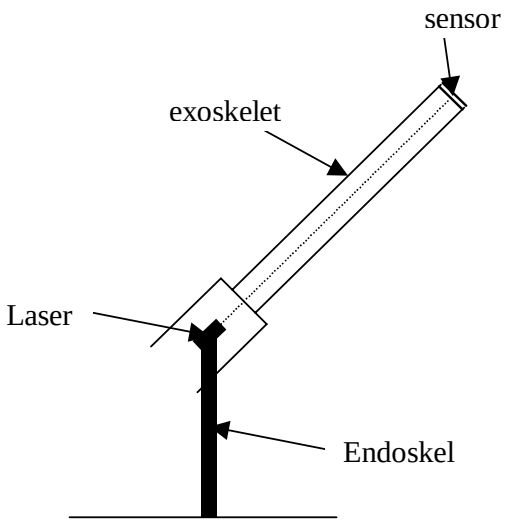

Figure 1 Schematic of laser guided arm

displacement with the laser light shining through the hollow robotic arm impinging upon a four-quadrant light intensity sensor mounted at the end of the arm. The sensor creates an error signal when the light spot is not at the centre of the sensor and guides the arm through the signal to the arm actuator system to move along the path.

The two-axis robot driven by two DC servo motors through harmonic drives [Lewis et a l 1995] stands (figure 2) on a heavy stone and metal

pedestal/socket with a supporting trunk made of Duralumin.

Figure 2 The flexible arm rig

The arm, which can move ±40º around the vertical and horizontal axes, can be changed so the system could be tested with arms of different stiffness and length. The robot control system consists of a master/slave relationship, with the master as the laser, which gives the direction and the robot arm is the slave. [Lewis 1996] Initial work by Lewis used a classical Proportional plus Derivative controller implemented on a PC. He produced a simple second order rigid model in MATLAB, which did not include the effects of flexibility and this gave poor predictions. [Surdhar 1999] used a fuzzy controller implemented on a Transputer array to achieve a much better performance.

1.2 Model of the Flexible robot

The following section dealing with the flexible arm is based on [White 1993] and [Sudhar 1999]. Similar techniques have been used elswhere [Tokhi et al 1997]. This technique was validated for simply supported and cantilever beams to within 1% of experimental measurements and classical analysis. Surdhar's use of a fuzzy controller does not rely on a model hence the problem of obtaining a non-minimum phase model or a highly accurate model is avoided. Nevertheless, a model is required to synthesise a controller to verify its stability and performance.

This model uses the finite difference technique applied to Euler-Lagrange formulation for a continuous shaft, which takes in account bending and shear moments to simulate the behaviour of a manipulator with a single flexible link.

The feedback from the tip of the arm via the tip-based sensor non-linear transfer function is included. The non-linear effects due to the motor current saturation limits are also included. Responses from higher vibration modes are filtered out in the practical implementation to prevent spillover. In order to simplify the model gravity effects are ignored. (The responses described later are in the horizontal plane). The equations for the arm and motor use standard Lagrangian description

It is assumed that the beam is small in diameter compared to its length, so that sections remain plane and translate but do not rotate. So effects of rotator inertia and of transverse shear deformation are neglected although they could be included. In figure 3 small displacements of the robot arm are shown.

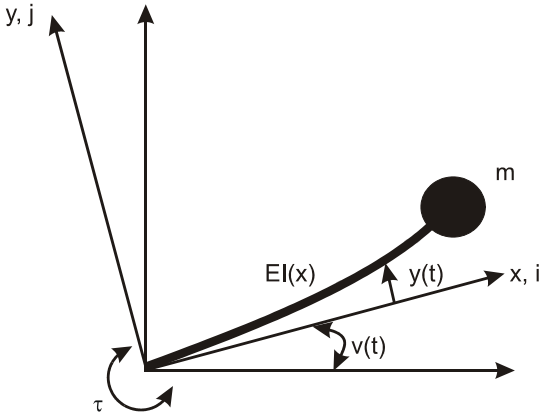

Figure 3 Deflection of the robot arm

Let a small segment of the arm be at a distance x from the origin. This is displaced by y(x,t).

Figure 4 shows the forces and moments on an element of length dx. The velocity v denotes the displacement at any section x at time t. M and S are the bending moment and the shear force at section x.

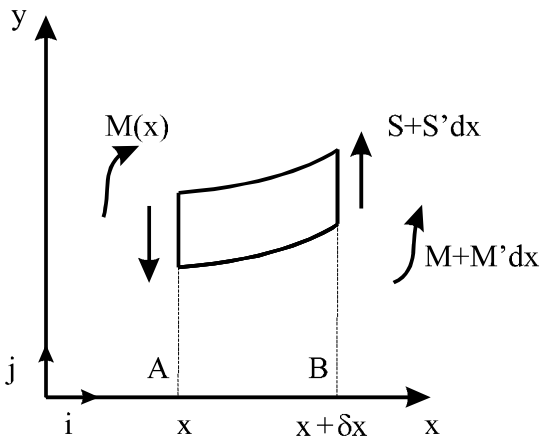

Figure 4 Elementary portion of the uniform beam

The mass of the segment is ρdx. At equilibrium the forces acting on the segment are:

$$\frac{\partial S}{\partial x} = \rho(\ddot{y} + x\dot{\omega}) \qquad (1)$$

hence

$$S = -\frac{\partial M}{\partial x} \tag{2}$$

From Euler's theory of bending using:

$$M = EI\frac{\partial^2 y}{\partial x^2} \tag{3}$$

From these we obtain

$$\rho(\ddot{y} + x\dot{\omega}) = -(EI\frac{\partial^4 y}{\partial x^4})(x,t) \tag{4}$$

Equation of motion for a segment of the arm rewriting equation 4:

$$\ddot{y} + \frac{1}{\rho}(EI\frac{\partial^4 x}{\partial x^4}(x,t)) = -x\dot{\omega} \tag{5}$$

The equation of the forces at the tip is:

$$m\dot{v} = \mathrm{m}(\ddot{y}(L,t) + L\dot{\omega}(t)) = -S(L,t) \tag{6}$$

While the equation of motion for a mass at the tip is derived as:

$$\frac{m}{\rho}\frac{\partial^4 y}{\partial x^4}(L,t) + \frac{\partial^3 y}{\partial x^3}(L,t) = 0 \tag{7}$$

The model solution is subject to the following boundary conditions:

The arm is fixed at the root:

$$y(0,t) = \frac{\partial y}{\partial x}(0,t) = 0 \tag{8}$$

Assuming the arm starts from rest initial conditions are:

$$\frac{\partial^2 y}{\partial x^2}(L,t) = 0 \tag{9}$$

For numerical solution using Advanced Continuous Simulation Language (ACSL) version 9 the central difference finite difference approximations and an explicit[1] method of solution is used [Smith 1985]:

$$y_n = \frac{y_{n+1} + y_{n-1}}{2}$$
$$\frac{\partial y}{\partial x}\Big|_n = \frac{y_{n+1} - y_{n-1}}{2\Delta x} \tag{10}$$
$$\frac{\partial^2 y}{\partial x^2}\Big|_n = \frac{y_{n+1} + y_{n-1} - 2y_n}{(\Delta x)^2}$$

The arm is divided into n stations, δx, as shown in figure 5.

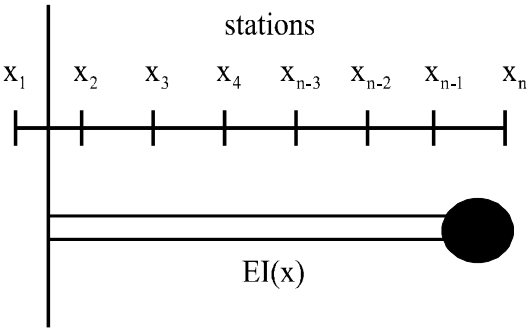

Figure 5 Finite difference segments

The boundary conditions derivative $\delta y/\delta x$ is represented accurately at x=0 and x=L through the central-difference approximation. In order to represent the boundary condition derivative $\delta y/\delta x$ more accurately at x=0 and x=L and to use the central-difference approximation, it is necessary to introduce 'fictitious' displacements. These have to correspond to y_{n-1} and y_{n+1}, which satisfy the boundary conditions, at the external mesh points by extending the arm slightly in a negative and positive direction. The length of the mesh is given by:

$$\delta x = \frac{L}{n-2} \tag{11}$$

L and n represent the length of the arm and number of stations respectively. The following boundary conditions are used:

$$y_1 = y_2 = 0;$$

$$M_{n-0.5} = 0; \quad \frac{M_n + M_{n-1}}{2} = 0$$

$$\frac{\partial^3 y}{\partial x^3}(L,t) = \frac{\partial M}{\partial x}\Big|_{n-0.5} = \frac{M_n - M_{n-1}}{dx} \tag{12}$$

Using a Taylor expansion the fictitious stations are eliminated and the following auxiliary quantity is obtained:

[1] a formula which expresses one unknown pivotal value directly in terms of known pivotal values

$$\frac{3h^3}{2}\frac{\partial^2 M}{\partial x^2}\Big|_{n-0.5} = 3M_n + M_{n-2} \qquad (13)$$

Substituting and using the boundary conditions in equation 12, the following solution is obtained:

$$M_n\left[1+\frac{M}{\rho Dx}\right] = -M_{n-2}\left[\frac{M}{3\rho Dx}\right] \qquad (14)$$

The explicit solution using the central difference approximation is stable for small integration times steps satisfying [Smith 1985]:

$$0 < \frac{\delta t}{(\delta x)^2} \le 0.5 \qquad (15)$$

The equation above implies that small integration time steps are required in the computer simulation. This constraint is easily satisfied in the simulation since δx=0.265 and δt=0.0001.

1.3 Motor and drive characteristics

The following equation gives the standard motor equations including the arm dynamics with the torque referred to the output shaft. [Dorf 1986][Kuo 1995]

$$\dot{\omega} = \frac{\tau}{NJ_e} - \frac{\omega\mu_e}{J_e} + \frac{EI}{N^2 J_e}\frac{\partial^2 M}{\partial x^2} \qquad (16)$$

Applying Kirchhoff's voltage law yields:

$$V_{app} = Ri + L\frac{di}{dt} + \omega(t)K_E \qquad (17)$$

The torque is generated by the armature, which moves in a permanent magnetic field. Manufacturers data shows that the torque is linearly related to the current.

$$\tau = K_T i \qquad (18)$$

The model of the sensor is derived from empirical data. The following figure 6 shows the experimentally obtained sensor transfer function by [Lewis 1996].

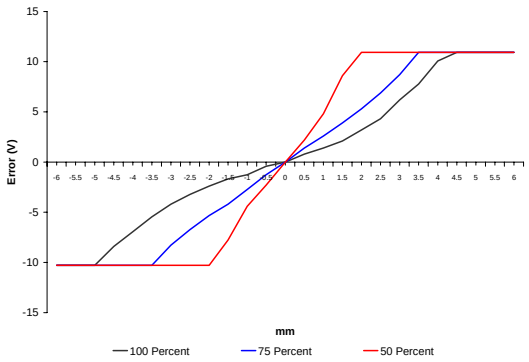

Figure 6 Measured sensor response for different spot sizes

The arm deflection is computed by the finite difference solution above in the following equation:

$$\Delta\theta = 1.5 * y_{n-1} - 0.5 * y_{n-2} \qquad (19)$$

The sum of the rigid body deformation, given by the hub angle, plus the tip deflection is the total displacement of the tip of the arm. Therefore the non-linear saturating function f_h transforms the deflection computation. The non-linear saturating function is modelled and it is included in the model. Equation 19 is redefined in the following equation 20 that describes the previous relationship and the error quantity:

$$e = \theta_c - (\theta + f_h\Delta\theta) \qquad (20)$$

The sensor maps the actual position error signal in X-Y space to a corresponding error voltage signal in the X (horizontal) and Y (vertical) plane. The X and Y error voltages are used to control the corresponding individual axes of the robot.

Under normal operation for the maximum load condition the sensor does not saturate. If the output voltage of the sensor exceeds 10 V sensor saturation is achieved. This means that the function in equation 20 can be approximated by a linear function. The magnitude of the largest deflection is 3.63 Volts and thus about 36% of the signal before saturation.

The gradient of f_h is K_{Tip}. It is the feedback parameter, which has been included as a conversion constant between the measured tip position (error) and its corresponding voltage, which is negatively fed back into the controller via a summing junction. In the simulation and practical experiments the value for K_{Tip} was kept constant at 3.3 V/mm.

Initially a table function was used to represent the sensor but proved to be unnecessary and a simple gradient was then used.

2.0 PARAMETERS OF THE MODEL

Table 1 shows the motor characteristics for combination of the DC motor and Harmonic Drive gears. Some data was obtained from the manufacturer* and some experimentally determined. [Pape & Korhonen 1995]

The motor current saturates at 1.9 A and this is the rated value as opposed to peak limits. As the datasheets specified gear efficiency, of 60% has also been included in the model

Table 2 summarises the measured structural parameters of the flexible aluminium arm.

Table 1 Motor Characteristics

Meaning:	**Value:**	**Unit:**
Voltage constant (B.E.M.F), motor	20.53	Vs/rad
Torque constant	0.26	Nm/A
Armature resistance	3.4	Ohm
Rated current	1.9*	A
Effective moment of inertia	0.00012*	kg m^2
Friction (viscous) of the system	0.00014*	kg m^2/ s

Table 2 Structural parameters

Parameter	**Description**	**Value**	**Unit (S.I)**
EI_m	Measured product of Young's modulus and 2^{nd} moment of inertia	8404 ±451	N m^2
EI_c	Calculated product of Young's modulus and 2^{nd} moment of inertia	8929±688	N m^2
ρ	Mass per unit length	0.75±0.0002	kg/m
m	Mass of tip sensor	0.15±0.0002	kg
L	Length of beam	1.18±0.005	m

The EI, the product of Young's modulus and the moment of inertia of the arm, was determined through measurements of the unloaded and loaded arm deflections and by use of Euler's beam theory.

2.2 Dynamic parameters of the arm

Table 3 and Table 4 summarise the measurements of the moments of inertia, J_{arm}, and viscous friction, μ_{arm}, of the robot arm for each axis of rotation. These measurements were made by [Pape 1995].

Table 3 Dynamic parameters for rotation about the horizontal axis of rotation

Parameter	Description	Value	Unit (S.I)
J_h	Moment of inertia, horizontal axis	0.22 ± 0.005	kg m^2
μ_h	Viscous friction, horizontal axis	0.127 ± 0.013	kg m^2/s

For the unloaded case there a series of measurements in the horizontal plane with different elevations, δ°, of the arm (cf. the experimental arrangement [Pape 1995]) were made.

The following Table 4 shows that there is a variation of up to 57.6% in the moment of inertia parameter and a variation of up to 43.5% in the viscous friction parameter for a variation in arm elevation of 0° to 40°. The ACSL simulation shown uses the parameters for 0° elevation

Table 4 Dynamic parameters for rotation about the vertical axis of rotation

Parameter	Description	Value	Elevation	Unit (S.I)
J_{arm}	Moment of inertia, vertical axis	0.639 ± 0.008	0°	kg m^2
J_{arm}	Moment of inertia, vertical axis	0.624 ± 0.008	9.8°	kg m^2
J_{arm}	Moment of inertia, vertical axis	0.271 ± 0.003	40.7°	kg m^2
μ_{arm}	Viscous friction, vertical axis	0.222 ± 0.004	0°	kg m^2/s
μ_{arm}	Viscous friction, vertical axis	0.218 ± 0.004	9.8°	kg m^2/s
μ_{arm}	Viscous friction, vertical axis	0.125 ± 0.002	40.7°	kg m^2/s

[Surdhar 1999] supposes that non-inclusion of the stiction and friction of the robot arm causes the difference between his original simulation values and the experimental data. Additionally the stiction and friction of the robot arm in this section will extend the present model. We will show here that this is not sufficient for a satisfactory explanation. Stiction and friction occurs at the supporting bearings. The Equation 20 has to be redefined:

$$\tau = K_T i - \tau_{in} \qquad (21)$$

τ_{out} is a stiction torque at the gear. Furthermore it is a factor, whose value depends on the direction in which the step response works.

Clockwise (RHS) stiction torque is 2.778 N m while the anticlockwise torque (LHS) is 0.926 N m. LHS denotes movements leftward about the

vertical motor axis looking out towards the arm and clockwise (RHS) denotes the opposite direction.

The measured stiction torque τ_{out} occurs at the gear, but to implement it in the program the stiction torque τ_{in} at the motor is needed. Therefore the equation 22 transforms the stiction torque at the gear in the stiction torque at the motor.

$$\tau_{out} = \tau_{in} * N \tag{22}$$

$$\omega_{out} = \frac{\omega_{in}}{N} \tag{23}$$

An if-loop in the program provides that the arm can only move if the motor torque is greater than the stiction torque.

2.4 Control

The error is defined as:

$$e = \theta_c - \theta \tag{24}$$

The control input under proportional control is:

$$u = K_p \cdot e \tag{25}$$

In practice a proportional plus derivative classical controller was used by Lewis and a Fuzzy PD controller used by Surdhar. Experiments using classical controllers applied to the tip feedback system (TFS) showed that PD control gave the best tracking and transient performance. The controllers were initially tuned by Zeiglers' method [Korhonen 1995 & Lewis 1995] with manual final tuning to achieve the best settling time compatible with the least overshoot.

The Fuzzy Controller is described in [Surdhar et al 2003]. The fuzzy algorithm was initially implemented in parallel on a single T800 transputer, but later on several T805 Transputers. Transputers were used because it was intended that this arrangement would be part of a much larger system operating on a parallel computer using a Transputer array at British Nuclear Fuels Plc.

The fuzzy architecture comprised 10 fuzzy sets for the antecedants (5 for error and 5 for derivative) and 5 output singletons. The aggregation of fired outputs was carried out by taking the sum of the fired elements and weighted average defuzzification was used to produce the crisp output. The principle reason for using a fuzzy controller is so that precise knowledge of the system is not required. In this case we are trying to predict how good the control is for a very complex structure. As will be seen later a good model of this structure was not simple to achieve.

The ASCL listing is completely described & listed in [Surdhar 1999]. It incorporates the fuzzy controller or classical PD controller; the flexible arm and motor current limits as well as the representation of friction and sensor characteristics.

2.5 Simulation

Both the Matlab and ACSL simulations can be run on any PC. The Matlab model took about 30 minutes to create and execute by an experienced user. The ACSL model took substantially longer to write since it uses terminal section Fortran statements to implement a search routine. Matlab is considerably easier to use and the more sophisticated model could have been cerated in Simulink. ACSL is line edited and compiled in the version used. Error correction is therefore more difficult than Matlab, which is interactive. ACSL allows more complex simulation to be executed but does not contain, in this version, any standard functions for this problem where simulation of partial differential equations was being executed. Matlab/Simulink is easier to use for novice users but ACSL is more robust and suitable for experienced programmers who have analogue computer knowledge.

3.0 MODEL VALIDATION

The following section describes a method to validate the simulation and shows the results of that ASCL simulation using step responses.
One method to validate the simulation results is the use of the correlation coefficient. [Neelamkavil 1981] These measures help to quantify the degree of relationship between two variables or their tendency to vary independently rather than together. There are two sets of data x_i and y_i. Both sets have n data. $\bar{x}$ and $\bar{y}$ are the average of the two sets of data. So the following Equation 26 calculates the correlation coefficient.

$$correl. = \frac{\sum (x_i - \bar{x})(y_i - \bar{y})}{\sqrt{\sum (x_i - \bar{x})^2 \sum (x_i - \bar{y})^2}} \qquad (26)$$

[Neelamkavil 1981] explains that the variable x_i and y_i are positively correlated if correl.>0 and here if x_i increase (decrease), y_i also tends to increase (decrease). When correl.<0, x_i and y_i are negatively correlated and if in this case one variable increases (decreases), the other variable is likely to decrease (increase). The variables x_i and y_i are perfectly correlated if correl.=1, they are uncorrelated when correl.=0.

For the the Matlab simulation of Lewis (figure 7) the simulation matched the prototype only 23% for the proportional control and 34% for the PD-control step response. Thus that simulation was not very useful.

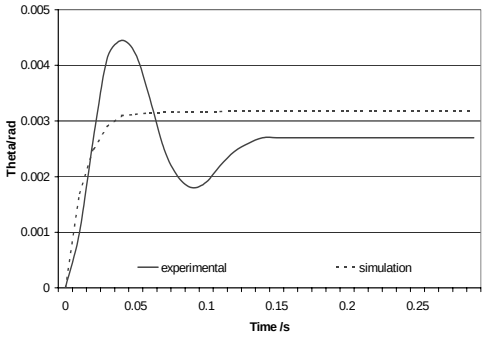

Figure 7 Lewis's simulated vs experimental results

Table 5 Correlation coefficient for clockwise rotation without stiction torque

Clockwise rotation				
time range/mass	**0 kg**	**0.7 kg**	**1.15 kg**	**1.6 kg**
0 s to 0.98 s	0.9432	0.8612	0.8251	0.7804

Table 6 Correlation coefficient for anti-clockwise rotation without stiction torque

Anticlockwise rotation			
time range/mass	**0.7 kg**	**1.15 kg**	**1.6 kg**
0 s to 1 s	0.8832	0.8915	0.8880

Tables 5 and 6 show the correlation coefficient for each direction without the stiction torque. For the clockwise movements with no payload and for the time range from 0 s to 0.98 s the correlation coefficient is 94 %. This is quite high. But the correlation coefficient decreases with more payload, because the simulation data sets do not change significantly as the reader can see from figure 8. For the anticlockwise movements the correlation coefficient is higher than for the clockwise movements.

The most significant observation is that clockwise the response is larger than the simulation and also

does not come to the desired value but leaves a steady state error. This is not the same for the anti-clockwise response.

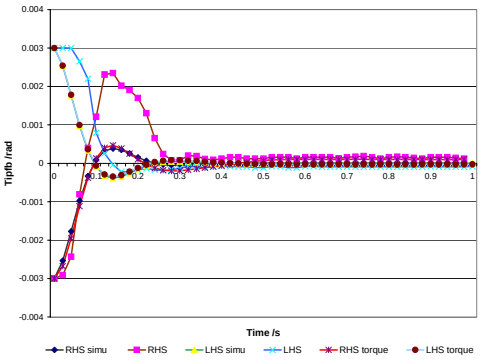

Figure 8 Measured values cf simulation without stiction

Table 7 Correlation coefficient of clockwise rotation with stiction torque

Clockwise motion with stiction torque				
time range/mass	**0 kg**	**0.7 kg**	**1.15 kg**	**1.6 kg**
0 s to 0.98 s	0.9233	0.8453	0.8166	0.5457

Tables 7 & 8 show the correlation coefficient of the simulation with included stiction torque. By adding the simulation with the stiction torque the correlation coefficients for the anti-clockwise direction increase only slightly for a 1.6 kg payload and in the time range from 0 s to 1 s. It is interesting that for 1.6 kg payload and the time range from 0 s to 0.98 s the correlation coefficient for the clockwise response drops from 78% to 54.6%.

Figure 9 shows the simulated step response with the included stiction torque for the clockwise movement. 'simu, mass=*, represent the simulation step response with the respective payloads and 'LHS' is an abbreviation for prototype. As the figure shows there are no differences between the simulated step responses despite different payloads. The same figure shows the anticlockwise step responses.

One experimental feature not reproduced by the model is the fundamental oscillations that appear at high tip loads. This is due to the aliasing filter being set too low to filter out the lowered vibration frequencies at higher loads. Incidentally this does not occur with the fuzzy controller.

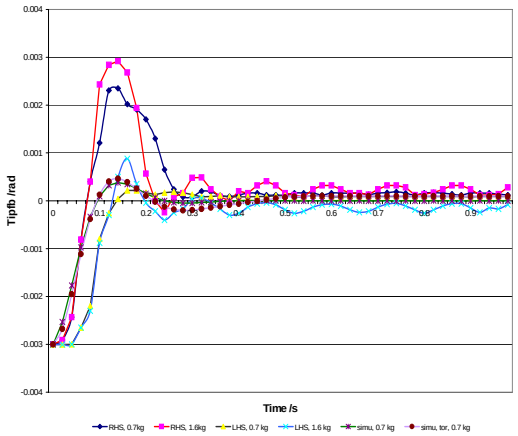

Figure 9 Effects of stiction torque compared to measured values

Table 8 Correlation coefficient of anticlockwise rotation with stiction torque

Anticlockwise motion with stiction torque			
time range/mass	**0.7 kg**	**1.15 kg**	**1.6 kg**
0 s to 1 s	0.8896	0.8945	0.8927

The correlation coefficient between the simulation and the prototype with fuzzy-control and 0 kg load for the anticlockwise direction is 0.9926. This is very good. Even with added loads it did not fall below 90%. As the reader can see in figure 10 there is only a time displacement between the both graphs. For the experimental values no significant difference occurrs in the two directions. There is still a small steady state error due to this not being heavily penalised in the fuzzy structure.

Tables 8 to Table 11 show the results of the peak percent overshoot, rise and settling time for the prototype for different payloads and the simulation with and without stiction torque. There are no significant differences between the characteristics of the simulation step responses with different payload as the reader can see in figures 8 & 9. Therefore only one rise and settling time and peak percent overshoot for the simulation with and without stiction torque in each direction is shown.

As the simulation result without stiction torque shows that the rise time is almost the same like it is for the left handside direction for 0.7 kg payload, but the rise time for the RHS movement is two times faster than the simulation. The settling times of the RHS response with 1.6 kg and LHS responses with 1.15kg and 1.6 kg are greater than 0.9 s , because they are more oscillatory.

The settling time for the RHS step response with stiction torque is almost two times greater than the LHS response and the response without stiction torque.

The peak percentage overshoot of the RHS step response for 0.7 kg payload is five times greater than the simulation and 20 times greater than the LHS step response. Besides the peak percent overshoot increase from 39% to 85% for the RHS step response and from 3.% to 20% for the LHS response with the increase of the payload from 0 kg to 1.6 kg.

Table 9 Characteristics of the prototype step response for clockwise rotation

Clockwise /load	**0 kg**	**0.7 kg**	**1.15 kg**	**1.6 kg**
T_r **/s**	0.03	0.03 s	0.045	0.03
T_s **/s**	0.3	0.29 s	0.33	>0.9
Overshoot %	38.5	67.7	94.7	84.9

Table 10 Characteristics of the prototype step response for anticlockwise rotation

Anticlockwise/ mass	**0.7 kg**	**1.15 kg**	**1.6 kg**
T_r **/s**	0.0623	0.0396	0.056
T_s **/s**	0.2751	>0.9	>0.9
Overshoot in %	3.38	25.4	20.35

Table 11 Characteristics of the simulation step responses for each direction

Simulation	**Without torque**	**Clockwise torque**	**Anticlockwise torque**
T_r **/s**	0.0682	0.0709	0.075
T_s **/s**	0.23672	0.5	0.375
Overshoot in %	12.7	12.64	10.0

The step response are shown typically for a payload of 0.7 kg because the simulation responses show no large differences with different payloads. To determine the source of these errors in overshoot and steady-state error a number of simulations were performed with a range of parameters using values which represent a wider range than was reasonably possible from the measured values. Effects of varying motor torque constant, viscous friction and different inertias on the system reponse were simulated. Of these only the inertia could yield overshoots as large as the measured response but would have to be damped by unusually large friction values. None can explain the steady state error.

3 2 Fuzzy Response

Table 12 shows the rise and settling time for the prototype and simulation for the right handside direction with fuzzy-control. Figure 10 gives the appropriate response. The shapes of the graphs look quite close. The simulation does not reach the 100% value of the prototype step response. Also there is a small time displacement between the two graphs.

Table 12 Characteristics of the step response with fuzzy control for RHS

Fuzzy-control	**Prototype**	**Simulation**
T_r /s	0.032	0.055

T_s /s	0.076	0.1

4.0 DISCUSSION

The correlation coefficient can be used to refute a simulation. Therefore the Matlab simulation is not a valid simulation of the behaviour of the flexible manipulator. For the ACSL simulation the correlation coefficients show that it is a useful simulation. The lowest coefficient without the additive stiction torque is 78% and the highest is 94%.

This makes it clear that the values of the data sets of the simulation and the prototype correlate very well at zero load. But if the reader compares the graphs they will be disappointed by the differences they can see. Through the added stiction torque in the program the correlation coefficients decrease for the RHS direction and rise only slightly for the LHS direction. The stiction torque was added to improve the performance of the simulation. The observed experimental response tests show a distinct difference between the step responses for the different directions and payloads in the overshoot. The peak percentage overshoot of the simulation with stiction torque decreases slightly and there are only small differences in the simulation between the peak percentage overshoot for the two directions. It is clear that the correlations for the second part of each response are poor because the measured responses are more oscillatory than the simulation. This would imply that the robot is more flexible than measured from static values. They also imply that this disparity is different in the two directions.

At the beginning of movement the motor torque is always so great that it can overcome the stiction torque. After this research it can be said that the stiction torque does not dominate the performance of the system.

Other effects that can cause different step responses for different payloads and different directions are the coulomb friction which is caused by the gearing and gear backlash. Both of them can be prevalent for practical systems but they are not modelled in this simulation as the harmonic drive exhibited no detectable backlash. The friction in the system was very close to the measured values.

After all these considerations and much effort expended on static calibration, there are only two aspects of the model that could cause such asymmetry. One is the stepper motor drive system for the laser. This was tested separately and did not exhibit such a tendency. The other possibility was the bolted joint connecting the arm tube section to the frame. If the small clearance in the bolt holes is considered and the direction of tightening is clockwise then a clockwise step input to the arm would tend to cause the bolts to slip but an anticlockwise step would tend to tighten the bolts. This movement only has to be of the order of 0.17 mm, which is comparable to the clearance in the holes.

The root stiffness of the arm is a significant factor in producing the oscillations seen in the records. Measurements of this effect are continuing.

5.0 CONCLUSION

The work of the simulation with Matlab shows how difficult the modelling of this project is, because this simulation is not good enough to represent the prototype.

This paper demonstrates the use of an ACSL program to simulate the prototype, modelling the continuous arm by means of finite difference terms. The correlation coefficient shows that the simulation is realistic but it is not recommended if it is used with different payloads and PD classical control.

The implementation of stiction torque to the simulation does not represent the phenomenon that the overshoot change depends on the direction and on the payload at the tip of the arm.

The use of this simulation to find a solution for the control problem for flexible robot arms using the fuzzy controller of Sudhar shows good results, because the correlation coefficient of the simulation with a fuzzy controller is 99% for 0 kg payload.

REFERENCES

Dorf, R C. 1986 "Modern Control Systems"; Addison-Wesley Publishing Company, Inc., United States of America.

Korhonen, J 1995 "Control and testing of a laser guided arm", MSc Project, Middlesex University, London.

Kuo, B C. 1995 "Automatic Control systems"; Prentice Hall, New Jersey.

Lewis, J 1996 "A Steady State Tip Control Strategy for Long Reach Robotics"; PhD thesis, Middlesex University, London.

Lewis, J, Gill, R & White, A 1995 "An Optical End-Point Position Control System for Long Reach Flexible Link Robots"; *The 11th ISPE/IEEE/IFAC*

International Conference on CAD/CAM Robotics and Factories of the Future'95.

Neelamkavil, F 1991 "Computer Simulation and Modelling"; John Wiley & Sons, Great Britain.

Pape, M. 1995 "An Investigation of the structural and dynamic properties of an optically guided robot arm"; Erasmus project, Middlesex University, London.

Smith., G D. 1985 "Numerical solution of partial differential equations"; Oxford University Press, New York.

Sudhar, J S: 1999 "Fuzzy PD Control of an Optically Guided Long Reach Robot". PhD thesis, Middlesex University, London,

Surdhar, J S & White, A S. 2003 "A parallel fuzzy controlled flexible manipulator using optical tip feedback", Robotics and Computer Integrated Engineering, 19, Pp273-282,.

Tokhi, M O, Mohamed, Z & Azad, A K M, 1997 "Finite difference and finite element approaches to dynamic modelling of a flexible manipulator"; Journal of Systems & Control Engineering, 211, 12, Pp 145-156, IMechE, London.

White A.S., 1993 'Simulation of Robot Vibrations,' IMA Conference on Robotics, Loughborough, 1989, Pp 553-558 July. reprinted in *Robotics: Applied Mathematics and Computational aspects*, Clarendon Press, ISBN 0-19-853649-6.

LIST OF SYMBOLS

Roman

e	error
EI	Young's modulus times second moment of area
i	current
J	Polar moment of inertia
K_e	constant
K_p	Proportional gain
K_T	Torque constant
L	Length of arm or inductance
M	Moment
N	Gear ratio
R	Armature resistance
S	Shear force
t	Time
T_r	Rise time
T_s	Settling time
v	Velocity
V_{app}	Voltage applied to armature
x	Distance along arm
y	Displacement of arm

Greek

δ	elevation of the arm
μ	Friction coefficient
θ	Hub rotation
ρ	Mass per unit length
τ	Torque
ω	angular velocity